Nanotextured PEDOT:Tos layers from block copolymer lithography

Florent Pawula, Solène Perrot, Georges Hadziioannou, Guillaume Fleury

Nanotextured PEDOT:Tos layers from block copolymer lithography

Florent Pawula*, Solène Perrot, Georges Hadziioannou, and Guillaume Fleury*

Univ. Bordeaux, CNRS, Bordeaux INP, LCPO, UMR 5629, F-33600, Pessac, France

*Corresponding authors:

florent.pawula@cnrs.fr, guilaume.fleury@u-bordeaux.fr

Abstract

Among functional materials, π-conjugated polymers are very attractive for large-scale or wearable applications thanks to their electronic and soft-matter properties. Poly(3,4-ethylenedioxythiophene) (PEDOT) based materials are often considered as the flagships of polymer electronics. Indeed, their tunable doping level affords various electronic transport behaviors, i.e. metallic, semi-metallic, or semi-conductor, with respect to the targeted applications. Furthermore, reducing the size of functional objects is a cornerstone of the semi-conductor industry's drive for improved performance. Hence, the nanopatterning of π-conjugated polymers and its relationship to electronic behavior is of high interest for future developments in polymer electronics. Here we report the texturation of PEDOT:Tos thin films at the nanometer scale *via* block copolymer lithography using self-assembled poly(styrene)-*block*-poly(methyl methacrylate) (PS-*b*-PMMA) layers as masks. By means of imaging and electronic spectral analyses, we demonstrate that doped-PEDOT nanostructures can be obtained

by this process through a re-doping treatment, enabling the recovery of the majority of the electronic states of the nanotextured PEDOT:Tos layer.

Introduction

π-conjugated polymers hold promise for the development of a novel generation of electronic devices with applications in the energy, sensing, or biomedical fields [1–3]. Among these materials, poly(3,4-ethylenedioxythiophene):poly(styrene sulfonate) (PEDOT:PSS) is one of the most intensively studied in organic electronics because of outstanding electronic properties and scalable fabrication processes based on printing technologies [4,5]. Other oxidants can be used to dope PEDOT chains generating PEDOT derivatives such as PEDOT:$FeCl_3$, PEDOT:ClO_4, PEDOT:PF_6, etc. One of particular interest is iron(III) p-toluenesulfonate (Tos) yielding to PEDOT:Tos with an inherent high electrical conductivity with respect to other π-conjugated polymer materials. Accordingly, the generation of functional nano-objects based on PEDOT:Tos is of high interest in the pursuit of miniaturization and performance of electronic devices. Within this context, we aimed at the modification of dimensionality and shape of PEDOT:Tos layers to generate ordered structures at the nanometer scale and to evaluate the interplay between electronic properties and nanostructuring. The manufacturing of the PEDOT:Tos nano-objects was performed by block copolymer (BCP) based nanolithography [6]. Indeed, nanostructured BCP thin films have been successfully used as masks to transfer a pattern into functional materials with potent demonstrations in the microelectronics industry [7–11]. The BCP masks were obtained using self-assembled poly(styrene)-*block*-poly(methyl methacrylate) (PS-*b*-PMMA) layers which afford fine control of the final pattern geometry due to the well-mastered self-assembling properties [6]. In particular, the similar surface energies of both blocks combined with the use of poly(styrene)-*stat*-poly(methyl methacrylate) (PS-*stat*-PMMA) grafted underlayers yields fine control of the BCP structure orientation [12]. Additionally, we further capitalize on the intrinsic selectivity of plasma chemistry between the PS and PMMA domains to etch with high fidelity the PEDOT:Tos layer [13,14]. Indeed, even if reactive ion etching RIE has been successfully used

to micro-pattern PEDOT:PSS [15,16], no attempt has been reported on the nano-texturation of PEDOT:Tos layers to the best of our knowledge. Hence, this study reports the texturing of PEDOT:Tos thin films at the nanometer scale using block copolymer lithography and the structural and electronic characterization of the resulting nanotextured films.

Experimental

Synthesis of PEDOT:Tos thin films

3,4-Ethylenedioxythiophene (EDOT) solution was purchased from TCI chemicals. The oxidant solution, 54 wt.% of Iron(III) p-toluenesulfonate ($Fe(Tos)_3$) in butanol (Heraeus Clevios CB54-V2), was used as a stock solution and modified with the addition of butanol to obtain the desired concentrations. Pyridine and DMSO were purchased from Acros Organics and Sigma Aldrich, respectively. All chemicals were used as received without further purification. Solutions containing 40 wt.% of tosylate were prepared with the addition of 0.5 mol of pyridine for 1 mol of $Fe(Tos)_3$. A high boiling point solvent (DMSO) was added in a volume fraction of 3 vol.% with respect to the oxidant solution volume. The solution was stirred for 12h at room temperature and then stored at 4°C. Microscope cover glasses purchased from Menzel-Gläser were used as substrate. The substrates were 15 × 30 mm² or 15 × 15 mm², contacted with gold (*vide infra*), and cleaned in isopropanol, ethanol, and acetone ultrasonic baths (10 minutes each) and blown dry with air.

As previously reported [17], *in situ* polymerization was performed by the addition of EDOT monomers to the $Fe(Tos)_3$ oxidant solution containing additives with an oxidant-to-monomer ratio equal to 2.3:1 (*i.e.* 2 mol of oxidant for the polymerization and 0.3 mol for the doping of the conjugated system). The solution was stirred for 5 s, filtered with a PTFE 0.22 µm filter and spin-coated on the substrate at 1500 rpm for 30 s, with a ramp of 800 $rpm.s^{-1}$. Films were

annealed at 100°C for 15 min. Finally, the films were allowed to cool down, washed in baths of 1-butanol and ethanol for 10 min, to remove the excess oxidant and additive, and blown dry with air.

Self-assembly of PS-b-PMMA thin films on top of PEDOT:Tos layers

The PS-*b*-PMMA and PS-*stat*-PMMA materials used in this study were obtained from Polymer Source and Arkema, respectively. The PS-*stat*-PMMA, synthesized by nitroxide-mediated radical polymerization using a SG1-based alkoxyamine, are end-functionalized with a hydroxyl group and a SG1 moiety, resulting in a grafting process involving both end-groups [18,19]. Propylene glycol methyl ether acetate (PGMEA) (Reagent Plus, 99.5%), was purchased from Merck and used as received. After washing the PEDOT:Tos thin films in a bath of PGMEA, a solution of PS-*stat*-PMMA (M_n = 13.4 kg.mol^{-1}, Đ = 1.38, f_{PS} = 0.52) at 2 wt.% in PGMEA was spin-coated at 1500 rpm on the PEDOT:Tos films. The sample was then annealed on a hot plate at 230°C for 5 min. A solution of PS-*b*-PMMA (M_n = 56.1 kg.mol^{-1}, Đ = 1.18, f_{PS} = 0.27) at 1.5 wt.% in PGMEA was subsequently spin-coated on top of the PEDOT:Tos layer at 2000 rpm, then annealed on a hot plate during 5 min at 290°C. A surface reconstruction step was performed by soaking the sample for 1 min in a 1:1 acetic acid:isopropanol solution. The process flow is summarized in **Figure 1**.

Nanolithography and doping process

In order to transfer the PS-*b*-PMMA pattern into the PEDOT:Tos layer, reactive ion etching (RIE) was performed on a capacitively-coupled plasma apparatus in parallel plate geometry with a working distance of 30 mm (13.56 MHz, FLRIE300-C, Plasmionique). Samples were treated with O_2 plasma (20 sccm) at 40 W for 90 s. Taking into account the 1:2 selectivity ratio between PS and PMMA [11,20], fine control of the plasma duration can yield to texturing of the PEDOT:Tos layer and removal of the BCP layer due to the similar etching speeds of PS and

PEDOT:Tos under the aforementioned conditions (see **Figure S2**). The textured PEDOT:Tos layer was then dipped in a 1M solution of sulfuric acid (H_2SO_4) for 10 min, washed in deionized water for 10 seconds, blown dry with air, and put on a hot plate at 100°C for 10 min [21].

Characterization methods

Atomic Force Microscopy (AFM) using a Dimension FastScan AFM (Bruker) in tapping mode with silicon cantilevers (FastScan-A, typical tip radius of ≈ 5 nm and resonance frequency of the cantilever of ≈ 1.25 kHz) was used to record the morphological features of films on intrinsic Si substrates. The root mean square roughness, R_q, was estimated from 2×2 μm^2 AFM images using Gwyddion software.

The thickness of the films was evaluated using a Bruker Dektak XT-A profilometer at several positions on the sample. The measurement was repeated at least three times at each position to yield the reported values with their respective standard deviations.

Scanning Electron Microscopy images were recorded with a JEOL 7800-E Prime microscope at room temperature under primary/high vacuum using the secondary electron detector (LED) at low acceleration voltage (1 or 2 kV) in the superhigh-resolution gentle beam mode (GBSH).

Electron spectroscopy measurements (X-Ray Photoelectrons Spectroscopy (XPS) and Ultraviolet Photoelectrons Spectroscopy (UPS)) were performed in a SPECS ultrahigh vacuum chamber at the ELORPrintTec platform (University of Bordeaux). For UPS, measurements were obtained using He(I) with a low-intensity UV light (21.22 eV). XPS measurements were performed using a monochromatized Al Kα X-ray source with an energy of 1486.6 eV. XPS spectra were fitted with the help of CasaXPS software. All the PEDOT:Tos films deposited on glass substrates were stored in a glove box before being analyzed by photoelectron spectroscopy to avoid environmental contaminations.

Based on XPS data, the effective doping level was calculated by considering the difference in the charge balance between anion and cation in order to normalize the spectral area. For PEDOT:Tos, the ratio of the oxidation states is 1, while this ratio is 1:2 for PEDOT:sulfate. Accordingly, a normalization of the integrals attributed to the sulfur atoms of the sulfate anion is necessary. The calculation of the doping level in a doped polymer with the ionized element in common (here S) can be generalized by the following equation:

$$Eff.Ox.level = \frac{m}{n} \frac{\int S(2p) \in B^{m-}}{\int S(2p) \in A}$$

with the hypothetical A^{n+}:B^{m-} couple, where *B* is the dopant of *A*.

Results and discussion

The main steps of the PEDOT:Tos texturing process are depicted in **Figure 1**. PEDOT:Tos was deposited on a glass substrate by *in situ* polymerization using an $Fe(Tos)_3$ oxidant solution at 40 wt.% in 1-butanol containing pyridine and DMSO as additives leading to a doping level of 22 ± 2% and a ≈ 55 nm thick film [17]. A cylinder-forming PS-*b*-PMMA with a PS volume fraction, f_{PS} = 0.27, was used as mask material to generate out-of-plane PS cylinders in a PMMA matrix (≈ 30 nm thick film) [22,23]. The control of the orientation of the BCP structure was achieved by depositing a thin PS-*stat*-PMMA layer on top of the PEDOT:Tos film (see **Figure S1**) in order to fine-tune the interfacial energies between the PEDOT:Tos and BCP domains [24,25]. Note that this step is mandatory in order to gain fine control of the PS-*b*-PMMA self-assembly resulting in the formation of out-of-plane PS cylinders. We believe that the formation of thermally-activated radicals at the SG1 chain end of the PS-*stat*-PMMA chains [19] is responsible for the efficient grafting on top of the PEDOT:Tos layer. The control of the orientation of the BCP structure was achieved by the deposition of PS-*stat*-PMMA chains

on top of the PEDOT:Tos film in order to finely tune the interfacial energies between the PEDOT:Tos and BCP layers. An O_2 plasma was then performed to transfer the BCP pattern into the PEDOT:Tos layer resulting in the formation of PEDOT:Tos nano-dots on the top of a PEDOT:Tos thin film. After the RIE treatment, the nanotextured PEDOT:Tos samples were redoped by soaking in a 1M solution of H_2SO_4 for 10 min before being washed in deionized H_2O, and post-baked at 100°C for 10 min.

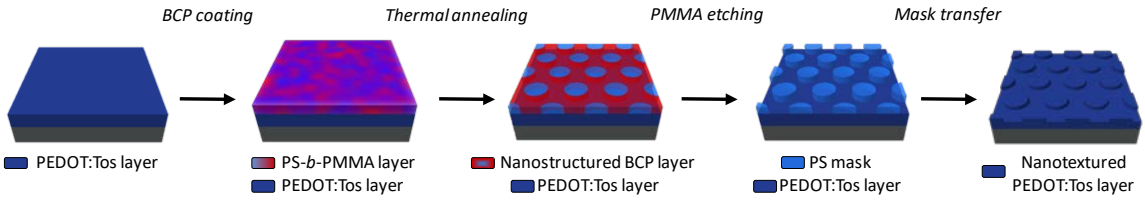

Figure 1. Process flow for nano-manufacturing of textured PEDOT:Tos thin film using self-assembled PS-*b*-PMMA film as a mask.

Topographical AFM images have been obtained at each step of the process. Firstly, pristine PEDOT:Tos films displayed the characteristic sponge-like structure of PEDOT:Tos film synthesized by *in-situ* polymerization as shown in **Figure 2a** [17]. After deposition of the BCP film and promotion of the self-assembly by thermal annealing, hexagonally packed PS cylinders with an out-of-plane orientation are formed even if the topographical contrast between the PS and PMMA domains is feeble (see **Figure 2b)**. This assignation is further confirmed through the surface reconstruction induced by soaking the sample in a 1:1 acetic acid:isopropanol solution leading to an increase in the topographical contrast between the PMMA and PS domains. From the AFM presented **Figure 2c**, the periodicity of the BCP structure was evaluated at 32.6 nm with a cylinder radius of 10.2 nm. Finally, the top panel of **Figure 2d** shows the resulting structure after the RIE treatment used to texture the PEDOT:Tos layer and to remove the BCP mask: an array of hexagonally packed PEDOT:Tos dots is clearly visible with a period of 35 nm and a cylinder radius of 11 nm, demonstrating the fidelity of the pattern

transfer. As shown in the bottom panel of **Figure 2d**, the redoping step using a H_2SO_4 treatment does not alter the PEDOT:Tos features with a pattern presenting similar geometrical characteristics as the one obtained after the RIE treatment. This behavior contrasts with reports on PEDOT:PSS films for which the formation of granular structures is observed upon H_2SO_4 treatment [26,27]. The structural integrity of the nanotextured PEDOT:Tos layers is related to the highly insoluble character of PEDOT:Tos films obtained after in-situ polymerization [28,29].

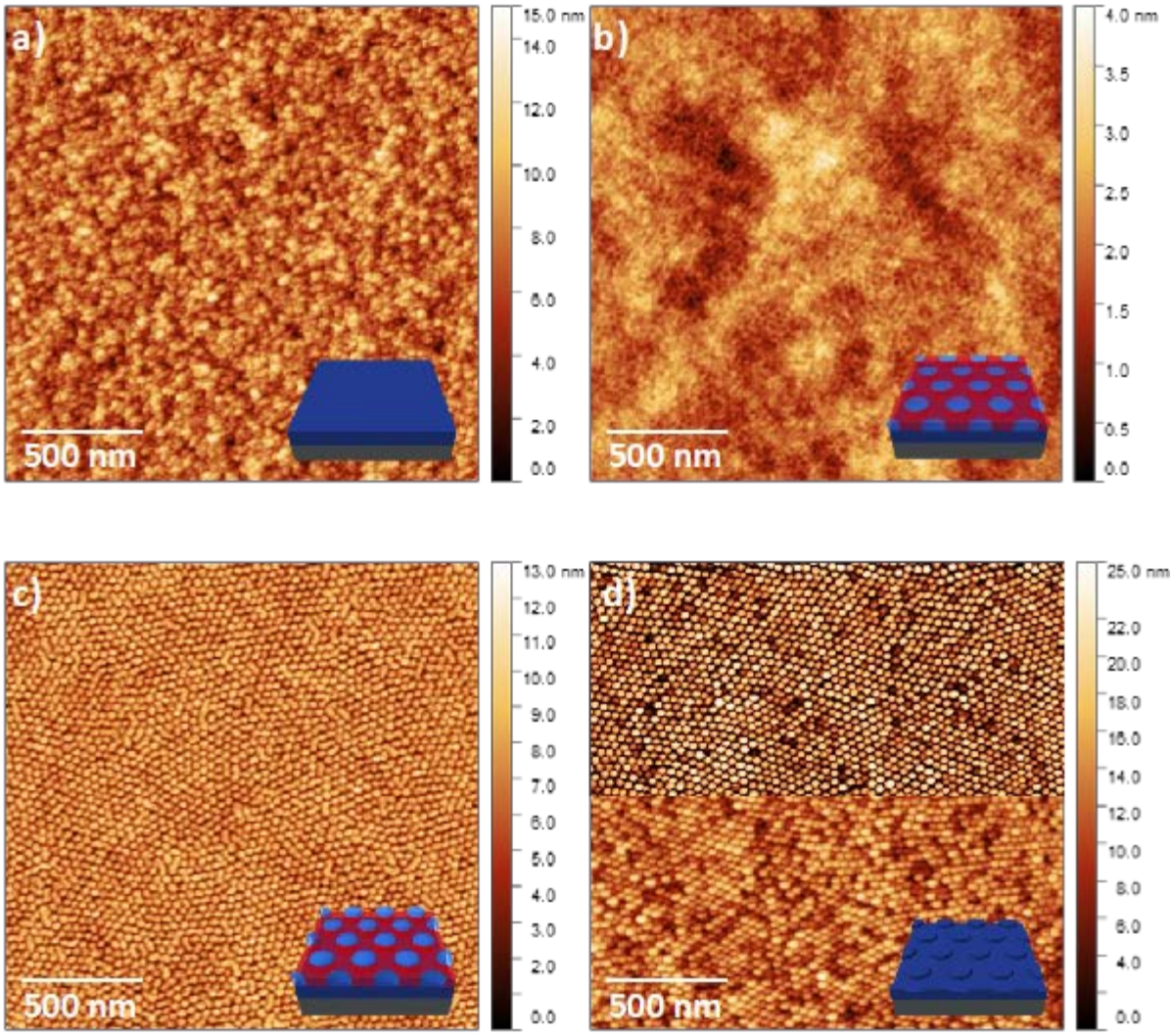

Figure 2. 2×2 μm^2 topographical AFM images of a) pristine PEDOT:Tos film, b) nanostructured PS-*b*-PMMA film on top of the PEDOT:Tos layer after thermal annealing, c) nanostructured PS-*b*-PMMA film after surface reconstruction in a 1:1 acetic acid:isopropanol solution, and d) the PEDOT:Tos dot array after etching (top panel) and after redoping in a H_2SO_4 solution (bottom panel).

The thickness of the textured PEDOT:Tos layer was evaluated at 44 nm, confirming the complete removal of the BCP mask at the end of the process. Topographical analysis of the surface demonstrated that the height of the dots is at least 14 ± 2 nm, as shown in **Figure 3**. Noteworthy, this value is consistent with the value extracted from the initial film thicknesses and etching speeds reported in **Figure S2**, i.e. *ca.* 15 nm.

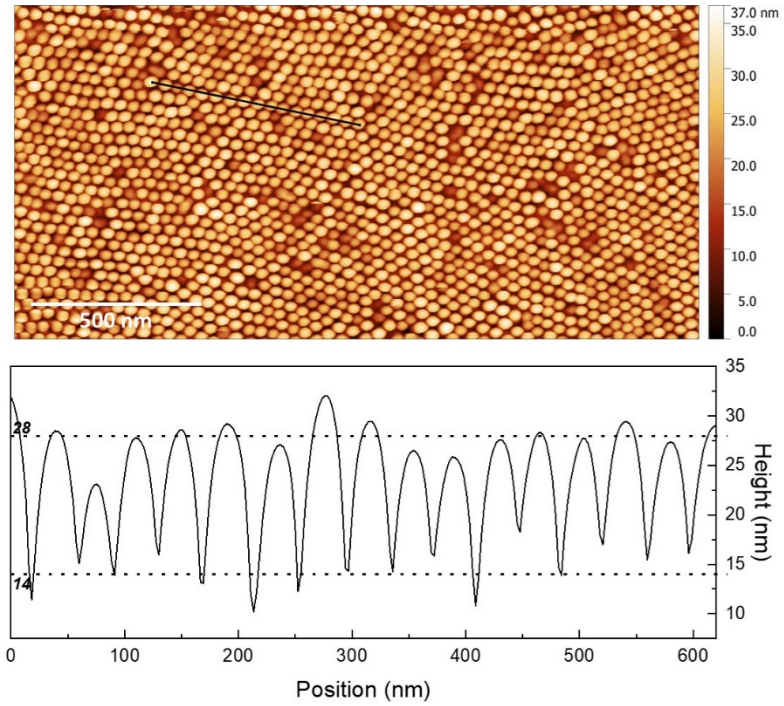

Figure 3. Topographical analysis of the textured PEDOT:Tos surface. (top) AFM topographical image and (bottom) height profile extracted along the black line. The standard deviation on the mean maxima and minima is 2 nm.

The texturation of the PEDOT:Tos layer was also evaluated by SEM as shown in **Figure 4**. The low magnification SEM image confirms the formation of hexagonally packed PEDOT:Tos dots over the whole surface and the stability of the structure after the redoping treatment by H_2SO_4.

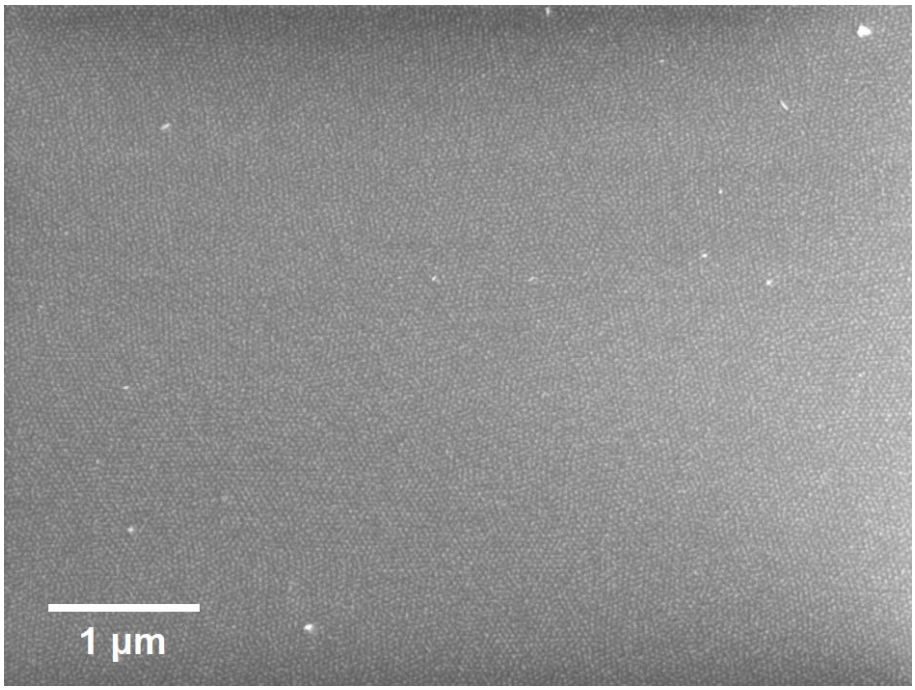

Figure 4. Low magnification SEM image of the array of PEDOT:Tos dots after redoping in a H_2SO_4 solution.

To investigate the electronic properties of the nanostructured PEDOT:Tos layer (and particularly the influence of the RIE and redoping treatments), the chemical composition of the PEDOT:Tos layer was established by analyzing XPS data for pristine, nanotextured, and redoped films. As expected, the survey spectrum of the samples showed the characteristic features of PEDOT:Tos with the 1s orbital of oxygen at 531 eV, the 1s orbital of carbon at 285 eV, and the 2s and 2p orbitals of sulfur at 229 eV and 165.5 eV (see **Figure S2**). For each chemical element, a high-resolution spectrum was recorded and finely analyzed to establish the composition. The XPS spectra are presented in **Figure 5** and the elementary ratios and oxidation levels extracted from XPS data are summarized in **Table 2**.

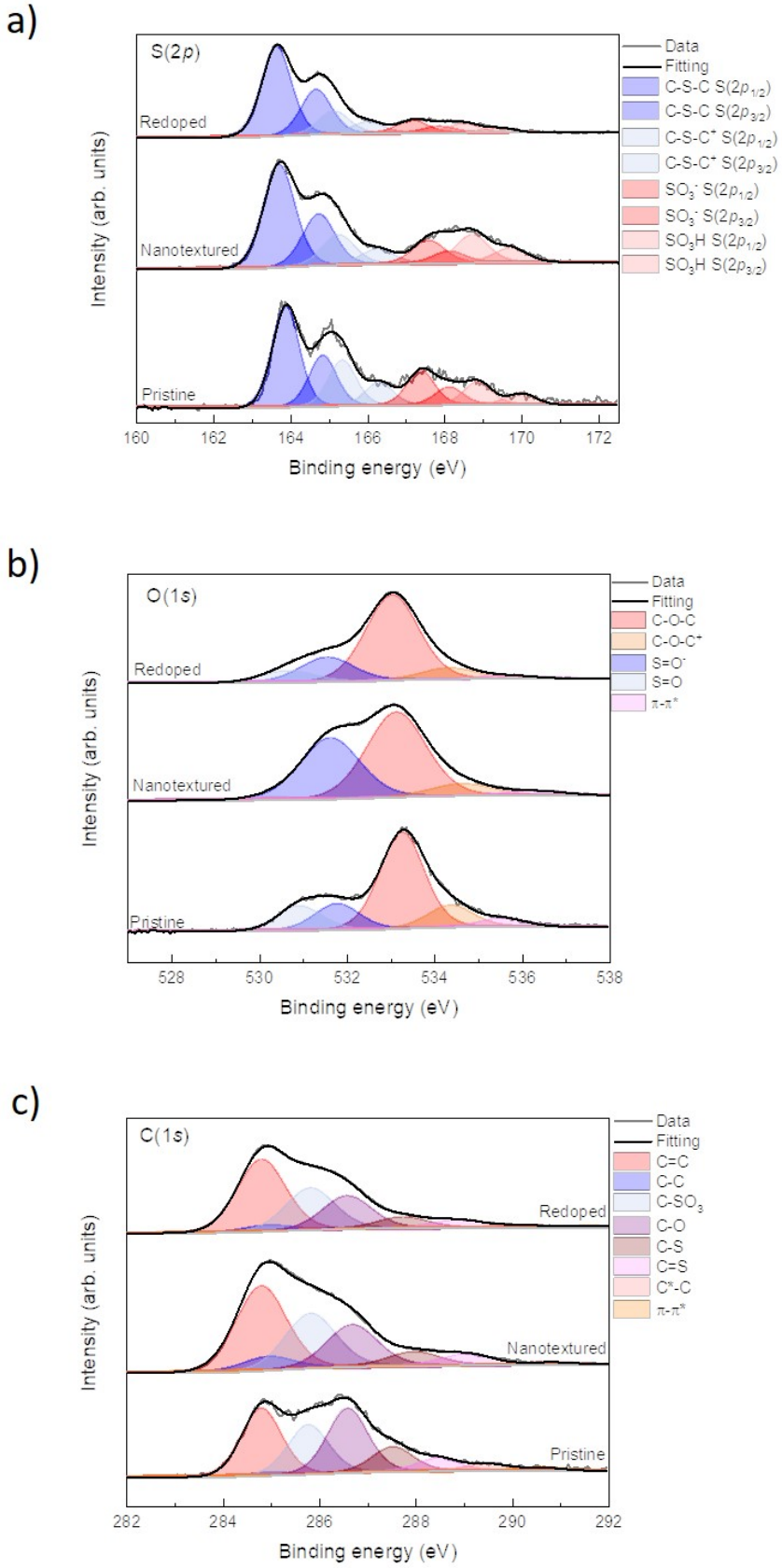

Figure 5. High-resolution XPS spectra of the a) S(2*p*), b) O(1*s*) and c) C(1*s*) orbitals for pristine, nanotextured, and redoped samples.

In the S(2*p*) orbitals spectra **Figure 5a**, the four doublets corresponding to the pristine sample are clearly observable in all samples around 163.7 eV, 165.3 eV, 167.4 eV, and 168.7 eV for S($2p_{1/2}$) of C-S-C, C-S-C^+, SO_3^-, and SO_3H respectively (see **Table 3** for the full description of the signal positions), ensuring the films are doped-PEDOT. As summarized in **Table 2**, the apparent doping level decreases along the process from 23.6% for the pristine sample, to 17.3% for the nanotextured one, to 11.1% after redoping. Nevertheless, these values should be carefully considered as the apparent doping level was calculated from the ratio between the area of the "S-O^-" signals (attributed to Tos^- for the pristine sample) and of the area of "C-S-C" and "C-S-C^+" signals (attributed to the thiophene and charged thiophene units of PEDOT, respectively) [30]. Indeed, it has been demonstrated that O_2 plasma chemistry can induce chemical side reactions through the formation of radicals and ions of high energy. In particular, Lui *et al.* reported the occurrence of C-O bond scissions in the PEDOT dioxy ring while the thiophene unit remains mostly stable under O_2 plasma chemistry [31]. Moreover, UPS spectra analysis hints the restoration of the electronic states close to the ones of the pristine sample after the redoping treatment (*vide infra*). Accordingly, anion exchange during the redoping treatment should be as well considered in order to accurately assess the doping level. Indeed, the redoping treatment by H_2SO_4 can lead to an exchange between the Tos^- and SO_4^{2-} anions, as already reported in the literature [28,32]. Consequently, an effective doping level has to be calculated based on a PEDOT:SO_4 complex leading to a doping level value twice as high as that calculated for a PEDOT:Tos complex, *i.e.* two negative charges on the SO_4^{2-} anion with respect to one negative charge on the Tos^- anion. Taking into account these considerations, an effective doping level depending on the type of PEDOT complexes was calculated which confirms the efficacy of the redoping procedure with an effective doping level of 22.2% for the nanostructured redoped PEDOT samples considering the formation of PEDOT:SO_4 complexes (see **Table 2**).

It is worth mentioning that, there is no consensus on the nature of the counter-anion following treatment by H_2SO_4 in the literature with reports mentioning HSO_4^- [26,33–35], SO_4^{2-} [28,32] or even a mixture of both anions [28]. An argument based on pKa values suggests that HSO_4^- is the main anion in water [34,35] but recent progress on the characterization of ionic mobility in hybrid perovskites have shown that the pKa values should be recomputed for a molecule in a bulk environment (relative to an aqueous solution) [36].

Table 1: Elementary ratios and oxidation levels extracted from XPS data and S(2*p*) spectra analysis, respectively. Ap. Ox. level and Eff. Ox. level are the apparent doping level (considering a PEDOT:Tos complex) and the effective doping level (considering a PEDOT:SO_4 complex), respectively.

	Pristine	Nanotextured	Redoped
O (%)	22.2	20.4	20.3
C (%)	55.3	62.3	63.6
S (%)	22.5	17.4	16.2
Ap. Ox. level (%)	23.6	17.3	11.1
Eff. Ox. level (%)	23.6	17.3	22.2

Additional hints on the formation of PEDOT:SO_4 complexes can be obtained by careful analysis of S(*2p*) binding energies along the nano-manufacturing process. The binding energy of all the S(*2p*) components decreases along the process except for the SO_3^- ($2p_{1/2}$) and SO_3^- ($2p_{3/2}$) components (see **Table 3**). After nanotexturing, the former increases while the latter remains constant. After redoping, both contributions decrease to slightly lower values than the ones of the pristine film. More importantly, the smaller binding energy values of those S(*2p*) orbitals in the redoped sample suggest that ionization of these sulfurs is easier, in accordance with the hypothesis of SO_4^{2-} as doping anion.

Compared to the pristine sample, the binding energy of the O(*1s*) components (corresponding to “C-O-C”, “$S=O^-$” and “S=O”) of the nanotextured and redoped films shift to lower energy (see **Table 3**). As opposed, the “$C\text{-}O\text{-}C^+$” and “$\pi\text{-}\pi^*$” binding energies of the nanotextured film shift to higher energy while the ones of the redoped film do not shift significantly. This means that the electronic environment of the oxygen in the dioxy ring “$C\text{-}O\text{-}C^+$” is rather similar to the one in the pristine film. Moreover, the ratio of the spectral area of the “$S=O/S=O^-$” is strongly reduced when nanotextured, from 0.94 to 0.05, and then increases upon acidic treatment up to 0.46, almost half the value of the pristine sample (see **Table S1**). This demonstrates the detrimental effect of the plasma and the beneficial effect of the redoping. Similarly, the “$S=O^-/C\text{-}O\text{-}C$” spectral ratio strongly increases upon the RIE process, from 0.27 to 0.72, and then decreases to 0.29, about the same value as for the pristine sample. All these observations are consistent with the hypothesis of the partial restoration of the electronic states as suggested above.

Concomitantly, the binding energy of the C(*1s*) in the dioxy ring of the redoped sample is the same as the pristine one. This means the electronic environment of this C is similar in both films, as observed for the O(*1s*). A similar analysis of the shifts of the binding energies is consistent with previous observations for S(*2p*) or O(*1s*) as C(*1s*) is bonded to one or the other.

To sum up, XPS spectra analyses support the presence of sulfate anions and suggest the partial recovery of the electronic states with an effective doping level for the redoped sample close to the pristine.

Table 2: Binding energies of the components of the XPS spectra.

Orbitals	Components	Binding energy (eV)		
		Pristine	Nanotextured	Redoped
C(*1s*)	C=C	284.8	284.8	284.8
	C-C	284.94	284.94	284.93
	C-SO_3	285.78	285.83	285.82
	C-O	286.59	286.69	286.58
	C-S	287.53	287.98	287.74
	C=S	288.48	289.08	288.89
	C*-C	289.53	290.84	290.21
	π-π*	290.65	292.91	291.61
O(*1s*)	C-O-C	533.27	533.14	533.05
	S=O^-	531.79	531.63	531.56
	S=O	530.91	530.25	530.65
	C-O-C^+	534.39	534.65	534.36
	π-π*	535.6	536.35	535.8
S(*2p*)	C-S-C ($2p_{1/2}$)	163.88	163.71	163.64
	C-S-C ($2p_{3/2}$)	164.85	164.75	164.68
	C-S-C^+ ($2p_{1/2}$)	165.36	165.26	165.14
	C-S-C^+ ($2p_{3/2}$)	166.31	166.28	166.02
	SO_3^- ($2p_{1/2}$)	167.39	167.6	167.17
	SO_3^- ($2p_{3/2}$)	168.13	168.13	167.86
	SO_3H ($2p_{1/2}$)	168.87	168.73	168.51
	SO_3H ($2p_{3/2}$)	170	169.72	169.45

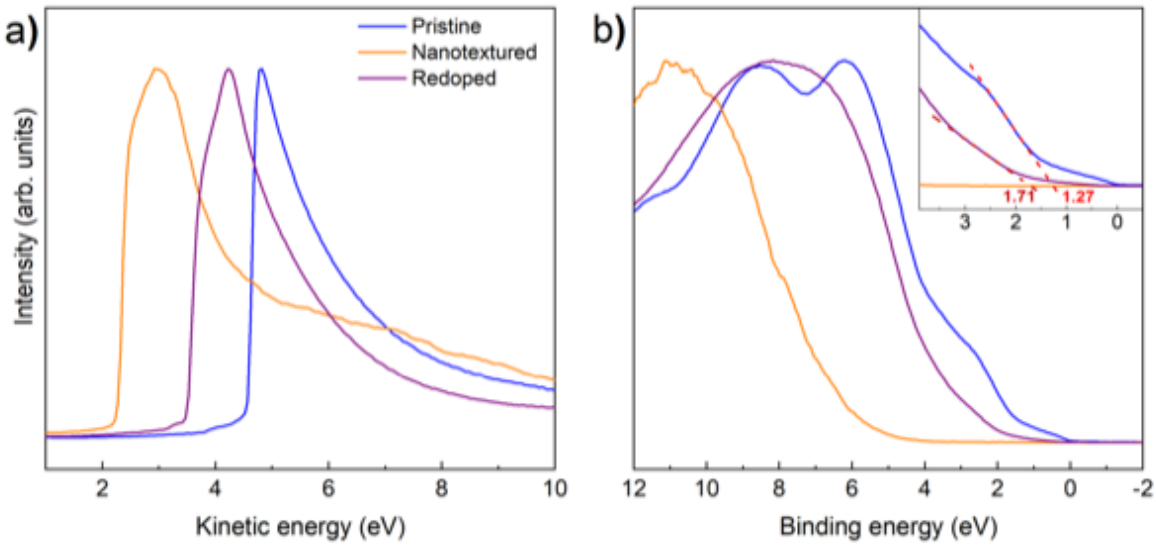

Figure 6: UPS spectra of pristine (blue), nanotextured (orange), and redoped (violet) PEDOT:Tos thin films. a) Secondary electron cut-off region showing the work function, and b) valence band region with a close-up at 0 eV in the inset displaying linear fits for estimating the HOMO level values. Binding energy equal to 0 eV represents the Fermi level.

The UPS spectra of the various samples are displayed **Figure 6**. The work function (WF) values are drastically modified during the texturing process: from 4.52 eV for the pristine sample, to 2.22 eV after pattern transfer, to 3.43 eV after redoping. As the WF is characteristic of the electronic state at the top surface of the sample, it is clear that the texturing process strongly modified the top surface. The WF values for PEDOT systems are influenced by, among others, doping level or chemical species at the top surface, e.g. segregation of PSS on top of the film in the case of PEDOT:PSS thin films [37,38]. Hence, the strong differences in the WF values observed here could arise from large variations in doping level (as retrieved from XPS analysis) and also probably from adsorbed residues related to the RIE treatment. In the valence band region displayed in **Figure 6b**, the spectral features are vastly different between the three probed samples. While small differences in the UPS spectra of PEDOT materials have been attributed to changes in crystallite orientation, morphology, or packing density [39,40], we did not consider these aspects to be dominant here. We opted to qualitatively compare the evolution

of the spectral features based on density functional theory calculations of the density of states (DOS) for PEDOT:Tos reported by Sharma et al. [41]. Accordingly, the spectral features at 2.6 eV and 6.2 eV arise from all the contributions, i.e. backbone, thiophene, dioxane, and randomly distributed tosylate, the small DOS at about 1 eV can be attributed to all contributions but dioxane, and the peak at ~ 8.5 eV can be attributed to all but tosylate. For the nanostructured sample, a large feature is visible around 11 eV and shifts upon redoping down to about 8 eV at a position close to the spectral features of the pristine PEDOT:Tos sample. Furthermore, the amount of electronic states at the Fermi level (see inset of **Figure 6b**), inherent to the semi-metallic character of doped PEDOT samples, vanishes completely during the pattern transfer by RIE, highlighting the strong modification of the electronic states at the surface induced by the O_2 plasma chemistry. More importantly, some of these electronic states appear to be recovered after redoping as demonstrated by the shift of the UPS spectra towards the Fermi level. Besides, a higher value of the highest occupied molecular orbital (HOMO) level is retrieved after redoping: 1.71 eV for the redoped nanotextured sample compared to 1.27 eV for the pristine one. This change is related to the ionization potential at the surface meaning that the top layer previously damaged by the plasma re-configures after acidic treatment. Such differences can be attributed to different surface morphologies, different crystallite orientations, etc. and it has been observed in PEDOT:Tos thin films, perylene-derivative and a,o-dihexyl-sexithiophene films [17,39,40]. Consistently, we speculate that the re-doping by SO_4^{2-} alters the conformation of the PEDOT chains as one SO_4^{2-} anion counterbalances two cationic PEDOT sites. Accordingly, even if the texturing process is detrimental to the electronic structure of the PEDOT:Tos layer, the redoping step leads to a partial recovery of electronic states involved in the charge transport mechanisms in PEDOT materials.

Conclusion

In this study, we demonstrate that nanostructured PS-*b*-PMMA films can be used to nano-texture PEDOT:Tos layers with high fidelity between the BCP mask and the resulting PEDOT:Tos structure. The process, derived from BCP lithography, enabled the formation of a hexagonal array of PEDOT dots with nanometric periodicity by using a cylinder-forming PS-*b*-PMMA BCP generating out-of-plane PS cylinders in a PMMA matrix. Nevertheless, the RIE treatment used to transfer the BCP pattern into the PEDOT:Tos layer yielded drastic modification of the PEDOT:Tos electronic properties with a decrease of the doping levels from 23.6% to 17.3%. To circumvent this issue, a redoping process based on the immersion of the PEDOT:Tos layer into an acidic H_2SO_4 bath was implemented to partially retrieve the electronic properties of the pristine PEDOT layer as attested by the increase of the doping level to a value close to the one of the pristine film assuming the formation of PEDOT:SO_4 complexes during the redoping step. The efficiency of the redoping step was further confirmed by UPS measurements as some of the characteristic semi-metallic states of doped PEDOT samples were recovered. We believe that the formation of a nanometric array of semi-metallic features holds promise for optical and electronic applications with the fundamental challenge to gain a deeper understanding on the relationships between the dimensionality and shape of π-conjugated polymer nano-objects, and their optical and electronic properties.

Acknowledgments

S. P. acknowledges financial support from the Région Aquitaine (PhD grant no. 2016-1R10206-00007195). The authors are grateful to the LabEx AMADEUS (ANR-10-LABEX-0042-AMADEUS) for financial support. This work was performed within the framework of the

EquipEx ELORPrintTec (ANR-10-EQPX-28-01) with the help of the French state Initiative d’Excellence IdEx (ANR-10-IDEX-003-02).

References

[1] A. Facchetti, *π-Conjugated Polymers for Organic Electronics and Photovoltaic Cell Applications*, Chem. Mater. **23**, 733 (2011).

[2] S. Inal, J. Rivnay, A.-O. Suiu, G. G. Malliaras, and I. McCulloch, *Conjugated Polymers in Bioelectronics*, Acc. Chem. Res. **51**, 1368 (2018).

[3] N. Kim, I. Petsagkourakis, S. Chen, M. Berggren, X. Crispin, M. P. Jonsson, and I. Zozoulenko, *Electric Transport Properties in PEDOT Thin Films*, in *Conjugated Polymers*, edited by J. R. Reynolds, B. C. Thompson, and T. A. Skotheim, 4th ed. (CRC Press, 2019), pp. 45–128.

[4] K. Sun, S. Zhang, P. Li, Y. Xia, X. Zhang, D. Du, F. H. Isikgor, and J. Ouyang, *Review on Application of PEDOTs and PEDOT:PSS in Energy Conversion and Storage Devices*, J. Mater. Sci. Mater. Electron. **26**, 4438 (2015).

[5] M. N. Gueye, A. Carella, J. Faure-Vincent, R. Demadrille, and J.-P. Simonato, *Progress in Understanding Structure and Transport Properties of PEDOT-Based Materials: A Critical Review*, Prog. Mater. Sci. **108**, 100616 (2020).

[6] C. M. Bates, M. J. Maher, D. W. Janes, C. J. Ellison, and C. G. Willson, *Block Copolymer Lithography*, Macromolecules **47**, 2 (2014).

[7] M. Park, C. Harrison, P. M. Chaikin, R. A. Register, and D. H. Adamson, *Block Copolymer Lithography: Periodic Arrays of ~10 ^{11} Holes in 1 Square Centimeter*, Science **276**, 1401 (1997).

[8] C. T. Black, K. W. Guarini, K. R. Milkove, S. M. Baker, T. P. Russell, and M. T. Tuominen, *Integration of Self-Assembled Diblock Copolymers for Semiconductor Capacitor Fabrication*, Appl. Phys. Lett. **79**, 409 (2001).

[9] K. W. Guarini, C. T. Black, K. R. Milkove, and R. L. Sandstrom, *Nanoscale Patterning Using Self-Assembled Polymers for Semiconductor Applications*, J. Vac. Sci. Technol. B Microelectron. Nanometer Struct. **19**, 2784 (2001).

[10] D. Zschech, D. H. Kim, A. P. Milenin, R. Scholz, R. Hillebrand, C. J. Hawker, T. P. Russell, M. Steinhart, and U. Gösele, *Ordered Arrays of 〈100〉-Oriented Silicon Nanorods by CMOS-Compatible Block Copolymer Lithography*, Nano Lett. **7**, 1516 (2007).

[11] R. A. Farrell, N. Petkov, M. T. Shaw, V. Djara, J. D. Holmes, and M. A. Morris, *Monitoring PMMA Elimination by Reactive Ion Etching from a Lamellar PS-* b *-PMMA Thin Film by* Ex Situ *TEM Methods*, Macromolecules **43**, 8651 (2010).

[12] P. Mansky, Y. Liu, E. Huang, T. P. Russell, and C. Hawker, *Controlling Polymer-Surface Interactions with Random Copolymer Brushes*, Science **275**, 1458 (1997).

[13] K. Asakawa and T. Hiraoka, *Nanopatterning with Microdomains of Block Copolymers Using Reactive-Ion Etching Selectivity*, Jpn. J. Appl. Phys. **41**, 6112 (2002).

[14] X. Gu, I. Gunkel, and T. P. Russell, *Pattern Transfer Using Block Copolymers*, Philos. Trans. R. Soc. Math. Phys. Eng. Sci. **371**, 20120306 (2013).

[15] B. Charlot, G. Sassine, A. Garraud, B. Sorli, A. Giani, and P. Combette, *Micropatterning PEDOT:PSS Layers*, Microsyst. Technol. **19**, 895 (2013).

[16] V. Kostianovskii, B. Sanyoto, and Y.-Y. Noh, *A Facile Way to Pattern PEDOT:PSS Film as an Electrode for Organic Devices*, Org. Electron. **44**, 99 (2017).

[17] S. Perrot, F. Pawula, S. Pechev, G. Hadziioannou, and G. Fleury, *PEDOT:Tos Electronic and Thermoelectric Properties: Lessons from Two Polymerization Processes*, J. Mater. Chem. C **9**, 7417 (2021).

[18] C. Navarro, S. Magnet, X. Chevalier, and R. Tiron, *Method For Preparing Surfaces*, WO2012140383 (18 October 2012).

[19] R. Chiarcos, V. Gianotti, M. Cossi, A. Zoccante, D. Antonioli, K. Sparnacci, M. Laus, F. E. Caligiore, and M. Perego, *Thermal Degradation in Ultrathin Films Outperforms Dose Control of N-Type Polymeric Dopants for Silicon*, ACS Appl. Electron. Mater. **1**, 1807 (2019).

[20] A. Sarrazin, N. Posseme, P. Pimenta-Barros, S. Barnola, A. Gharbi, M. Argoud, R. Tiron, and C. Cardinaud, *PMMA Removal Selectivity to Polystyrene Using Dry Etch Approach*, J. Vac. Sci. Technol. B Nanotechnol. Microelectron. Mater. Process. Meas. Phenom. **34**, 061802 (2016).

[21] S. Chen et al., *Conductive Polymer Nanoantennas for Dynamic Organic Plasmonics*, Nat. Nanotechnol. **15**, 35 (2020).

[22] M. W. Matsen and M. Schick, *Stable and Unstable Phases of a Diblock Copolymer Melt*, Phys. Rev. Lett. **72**, 2660 (1994).

[23] M. W. Matsen and F. S. Bates, *Unifying Weak- and Strong-Segregation Block Copolymer Theories*, Macromolecules **29**, 1091 (1996).

[24] D. G. Walton, G. J. Kellogg, A. M. Mayes, P. Lambooy, and T. P. Russell, *A Free Energy Model for Confined Diblock Copolymers*, Macromolecules **27**, 6225 (1994).

[25] E. Huang, S. Pruzinsky, T. P. Russell, J. Mays, and C. J. Hawker, *Neutrality Conditions for Block Copolymer Systems on Random Copolymer Brush Surfaces*, Macromolecules **32**, 5299 (1999).

[26] N. Kim, S. Kee, S. H. Lee, B. H. Lee, Y. H. Kahng, Y.-R. Jo, B.-J. Kim, and K. Lee, *Highly Conductive PEDOT:PSS Nanofibrils Induced by Solution-Processed Crystallization*, Adv. Mater. **26**, 2268 (2014).

[27] Y. Shi, Y. Zhou, R. Shen, F. Liu, and Y. Zhou, *Solution-Based Synthesis of PEDOT:PSS Films with Electrical Conductivity over 6300 S/cm*, J. Ind. Eng. Chem. **101**, 414 (2021).

[28] J. Wang, K. Cai, and S. Shen, *Enhanced Thermoelectric Properties of Poly(3,4-Ethylenedioxythiophene) Thin Films Treated with H_2SO_4*, Org. Electron. **15**, 3087 (2014).

[29] J. Wang, K. Cai, H. Song, and S. Shen, *Simultaneously Enhanced Electrical Conductivity and Seebeck Coefficient in Poly (3,4-Ethylenedioxythiophene) Films Treated with Hydroiodic Acid*, Synth. Met. **220**, 585 (2016).

[30] M. Fabretto, M. Müller, K. Zuber, and P. Murphy, *Influence of PEG*- Ran -*PPG Surfactant on Vapour Phase Polymerised PEDOT Thin Films*, Macromol. Rapid Commun. **30**, 1846 (2009).

[31] C. Liu, M. J. Goeckner, and A. V. Walker, *Plasma Polymerization of Poly(3,4-Ethylenedioxyethene) Films: The Influence of Plasma Gas Phase Chemistry*, J. Vac. Sci. Technol. Vac. Surf. Films **35**, 021302 (2017).

[32] Y. Li, X. Hu, S. Zhou, L. Yang, J. Yan, C. Sun, and P. Chen, *A Facile Process to Produce Highly Conductive Poly(3,4-Ethylenedioxythiophene) Films for ITO-Free Flexible OLED Devices*, J Mater Chem C **2**, 916 (2014).

[33] Z. Fan, P. Li, D. Du, and J. Ouyang, *Significantly Enhanced Thermoelectric Properties of PEDOT:PSS Films through Sequential Post-Treatments with Common Acids and Bases*, Adv. Energy Mater. **7**, 1602116 (2017).

[34] S. R. S. Kumar, N. Kurra, and H. N. Alshareef, *Enhanced High Temperature Thermoelectric Response of Sulphuric Acid Treated Conducting Polymer Thin Films*, J. Mater. Chem. C **4**, 215 (2016).

[35] Y. Xia, K. Sun, and J. Ouyang, *Solution-Processed Metallic Conducting Polymer Films as Transparent Electrode of Optoelectronic Devices*, Adv. Mater. **24**, 2436 (2012).

[36] D. R. Ceratti, A. Zohar, R. Kozlov, H. Dong, G. Uraltsev, O. Girshevitz, I. Pinkas, L. Avram, G. Hodes, and D. Cahen, *Eppur Si Muove: Proton Diffusion in Halide Perovskite Single Crystals*, Adv. Mater. **32**, 2002467 (2020).

[37] J. Huang, P. F. Miller, J. S. Wilson, A. J. de Mello, J. C. de Mello, and D. D. C. Bradley, *Investigation of the Effects of Doping and Post-Deposition Treatments on the Conductivity, Morphology, and Work Function of Poly(3,4-Ethylenedioxythiophene)/Poly(Styrene Sulfonate) Films*, Adv. Funct. Mater. **15**, 290 (2005).

[38] A. M. Nardes, M. Kemerink, M. M. de Kok, E. Vinken, K. Maturova, and R. A. J. Janssen, *Conductivity, Work Function, and Environmental Stability of PEDOT:PSS Thin Films Treated with Sorbitol*, Org. Electron. **9**, 727 (2008).

[39] S. Duhm, G. Heimel, I. Salzmann, H. Glowatzki, R. L. Johnson, A. Vollmer, J. P. Rabe, and N. Koch, *Orientation-Dependent Ionization Energies and Interface Dipoles in Ordered Molecular Assemblies*, Nat. Mater. **7**, 326 (2008).

[40] P. Sehati, S. Braun, and M. Fahlman, *Energy Level Alignment in Au/Pentacene/PTCDA Trilayer Stacks*, Chem. Phys. Lett. **583**, 38 (2013).

[41] A. Sharma, G. Andersson, J. Rivnay, J. F. Alvino, G. F. Metha, M. R. Andersson, K. Zuber, and M. Fabretto, *Insights into the Oxidant/Polymer Interfacial Growth of Vapor Phase Polymerized PEDOT Thin Films*, Adv. Mater. Interfaces **5**, 1800594 (2018).